

## RESEARCH ARTICLE

# Miniature intravascular photoacoustic endoscopy with coaxial excitation and detection

Riqiang Lin<sup>1,2</sup> | Qi Zhang<sup>1</sup> | Shengmiao Lv<sup>2</sup> | Jiaming Zhang<sup>1</sup> |  
Xiatian Wang<sup>2</sup> | Dongliang Shi<sup>1</sup> | Xiaojing Gong<sup>2</sup>  | Kwok-ho Lam<sup>1,3</sup> 

<sup>1</sup>Department of Electrical Engineering, The Hong Kong Polytechnic University, Kowloon, Hong Kong

<sup>2</sup>Research Center for Biomedical Optics and Molecular Imaging, Shenzhen Key Laboratory for Molecular Imaging, Guangdong Provincial Key Laboratory of Biomedical Optical Imaging Technology, CAS Key Laboratory of Health Informatics, Shenzhen Institute of Advanced Technology, Chinese Academy of Sciences, Shenzhen, China

<sup>3</sup>Centre for Medical and Industrial Ultrasonics, James Watt School of Engineering, University of Glasgow, Glasgow, Scotland, UK

## Correspondence

Kwok-ho Lam, Centre for Medical and Industrial Ultrasonics, James Watt School of Engineering, University of Glasgow, Glasgow, Scotland, UK.

Email: [kwokho.lam@glasgow.ac.uk](mailto:kwokho.lam@glasgow.ac.uk)

Xiaojing Gong, Shenzhen Institute of Advanced Technology, Chinese Academy of Sciences, Shenzhen 518055, China.

Email: [xj.gong@siat.ac.cn](mailto:xj.gong@siat.ac.cn)

## Funding information

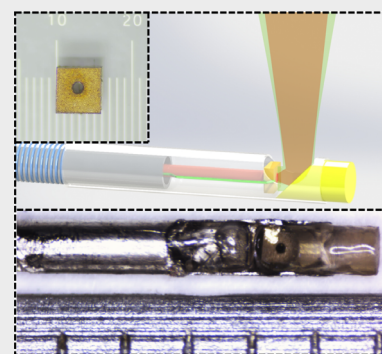
Guangdong Provincial Key Laboratory of Biomedical Optical Imaging Technology, Grant/Award Number: 2020B121201010; Hong Kong Research Grants Council, Grant/Award Number: 15220920; Hong Kong Research Impact Fund, Grant/Award Number: R5029-19; National Key Research and Development Program of China, Grant/Award Number: 2018YFC0116300; National Natural Science Foundation of China, Grant/Award Numbers: 61975226, 62005306; Shenzhen Science and Technology Innovation Committee, Grant/Award Numbers: JCYJ20200109114610201, ZDSY20130401165820357; CAS Key Laboratory of Health Informatics, Grant/Award Number: 2011DP173015

## Abstract

Recent research pointed out that the degree of inflammation in the adventitia could correlate with the severity of atherosclerotic plaques. Intravascular photoacoustic endoscopy can provide the information of arterial morphology and plaque composition, and even detecting the inflammation. However, most reported work used a noncoaxial configuration for the photoacoustic catheter design, which formed a limited light-sound overlap area for imaging so as to miss the adventitia information. Here we developed a novel 0.9 mm-diameter intravascular photoacoustic catheter with coaxial excitation and detection to resolve the aforementioned issue. A miniature hollow ultrasound transducer with a 0.18 mm-diameter orifice in the center was successfully fabricated. To show the significance and merits of our design, phantom and ex vivo imaging experiments were conducted on both coaxial and noncoaxial catheters for comparison. The results demonstrated that the coaxial catheter exhibited much better photoacoustic/ultrasound imaging performance from the intima to the adventitia.

## KEYWORDS

coaxial catheter, ex vivo, intravascular, photoacoustic endoscopy



This is an open access article under the terms of the [Creative Commons Attribution-NonCommercial-NoDerivs](https://creativecommons.org/licenses/by-nc-nd/4.0/) License, which permits use and distribution in any medium, provided the original work is properly cited, the use is non-commercial and no modifications or adaptations are made.

© 2022 The Authors. *Journal of Biophotonics* published by Wiley-VCH GmbH.

## 1 | INTRODUCTION

Atherosclerosis is a chronic inflammatory disease [1, 2], which is mainly characterized by plaques [3, 4] and inflammation [5, 6] developed inside the arterial wall. Rupture of vulnerable plaque in atherosclerosis is the leading cause of acute cardiovascular events [7]. Early detection and identification of vulnerable plaque are crucial to prevent acute coronary syndromes [8–10]. Previously, research efforts focused on the imaging of artery intima where the plaque and inflammation generated. Some recent work revealed that the situation of inflammatory cells in the adventitia correlates with the severity of atherosclerotic plaques [11–13]. In addition, the formation of adventitial tertiary lymphatic organs (ATLOs), which are well-organized structures with areas of T cells, B cells and antigen-presenting cells, has been associated with atherosclerosis in mice [13, 14]. It has been proven that ATLOs are able to establish an artery-brain circuit, which can help to slow down disease progression and improve plaque stability [15]. Thus, the information in the tunica adventitia is important for diagnosis and remedy of atherosclerosis.

Intravascular photoacoustic imaging has been proven as one of effective tools for the assessment of plaque [16–19]. Various designs of photoacoustic catheters were developed [20–23], in which most reported catheters induced a limited overlap area to image with either oblique illumination and side-view detection or oblique detection and side-illumination, providing the effective excitation and detection in artery intima. The imaging results of lipid in the preadventitia were reported [24–26]. However, the noncoaxial design used a big fiber core to irradiate the target, causing lower optical fluence and demanding higher energy.

An alternative design is coaxial optical excitation and ultrasound detection [27–31]. The first coaxial photoacoustic endoscopic probe was reported in 2011, in which a hollow ultrasound transducer was with an outer diameter of 2.2 mm [27]. In 2014, another coaxial probe with a 2.9 mm-diameter transducer was developed for a high-speed photoacoustic system [28]. In 2016, a hollow structured lens-focused transducer with an outer diameter of 7 mm was developed [29]. All aforementioned endoscopic probes were with good performance in photoacoustic imaging. However, these probes were too bulky for use in tiny cardio vessels. In 2016, a multimode fiber with a 45° polished distal end was designed to irradiate the laser and reflect the photoacoustic signals [30, 31]. The diameter of this probe was down to 1 mm, but the photoacoustic signal collection depended on the surface of a 400  $\mu\text{m}$ -diameter optical fiber. The miniature aperture of the fiber could not cover the aperture of the ultrasound transducer, leading to weak detection and low signal-to-noise ratio (SNR).

The diameter of human coronary arteries is in the range of 1.5–5.6 mm [32]. To ensure passing through the intravascular vessel, the clinical intravascular catheter dimension is limited to be <1 mm. In this study, a miniature 0.9 mm-diameter catheter employing coaxial optical illumination and ultrasonic detection was developed, which promised a large imaging depth from the intima to the adventitia. A 0.6 mm  $\times$  0.6 mm  $\times$  0.4 mm PZT-5H-based hollow ultrasound transducer with an  $\sim$ 0.18 mm-diameter orifice was successfully fabricated. A multimode fiber with a 0.105 mm-diameter core was inserted through the orifice, forming the coaxial design. A rod mirror was employed for reflecting laser and photoacoustic waves, which was with the area of  $\sim$ 4 times larger than the previous fiber core, fully covering the transducer aperture. The catheter performance was evaluated by imaging tungsten wires, which showed that the coaxial configuration acquired better imaging depth when compared with the noncoaxial design of our previous work [33]. Moreover, the ex vivo imaging of nanoprobe, mimicking the targeted cells at the adventitia of porcine coronary artery, was acquired using the developed miniature catheter to demonstrate the imaging capability for future clinical research.

## 2 | METHODS AND MATERIALS

### 2.1 | Preparation of hollow ultrasound transducer

Ultrasound transducer is an important element in this work, in which the frequency is generally 20–45 MHz. To meet the clinical demand, our targeted catheter dimension is 0.9 mm with the ultrasound frequency of 30–35 MHz and the bandwidth of 40%. A 10 mm  $\times$  10 mm 30-MHz acoustic stack based on PZT-5H ceramics (CTS Corporation, USA) was prepared using the conventional transducer technology [34, 35] as shown in Figure 1A. The

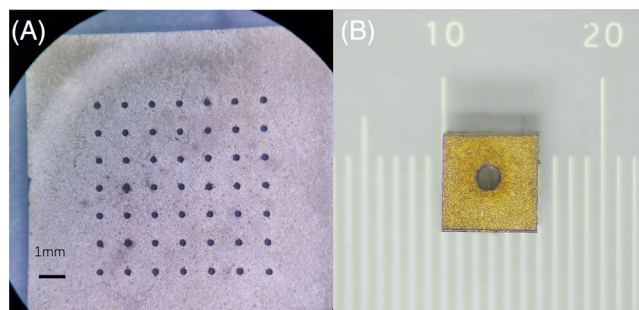
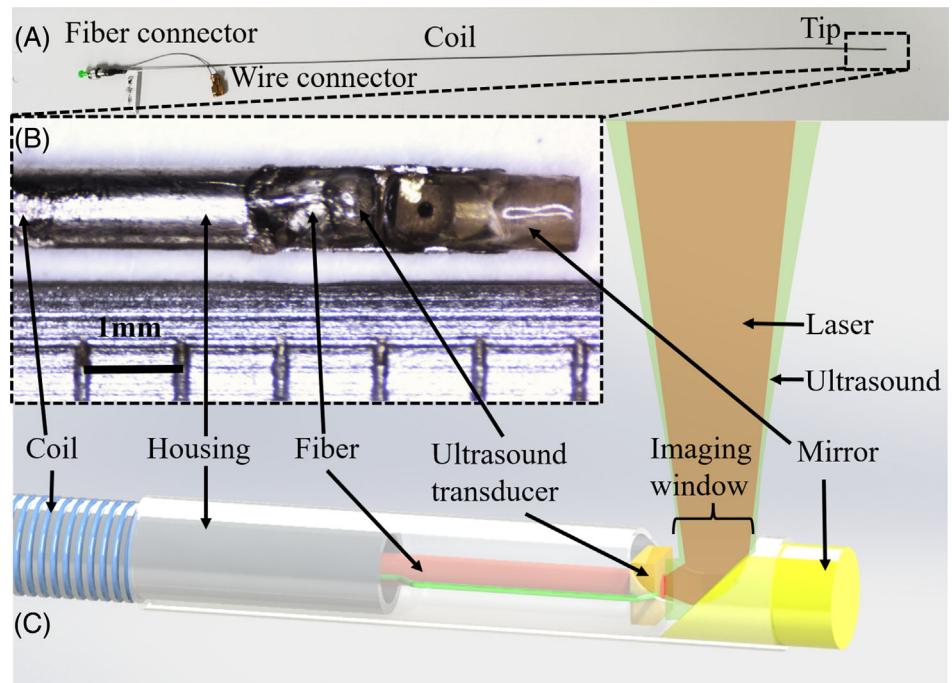


FIGURE 1 (A) Photo of a 10 mm  $\times$  10 mm acoustic stack with 49 orifices; (B) photo of a 0.6 mm  $\times$  0.6 mm  $\times$  0.4 mm hollow acoustic stack with a  $\sim$ 0.18 mm-diameter central orifice

**FIGURE 2** Photos and schematic of the coaxial intravascular photoacoustic catheter. (A) Photo of the whole catheter; (B) zoom-in photo of the tip of the catheter; (C) schematic of a 3D model of the catheter



center orifice was for laser beam delivery, which was set as 0.18 mm to enable the fiber core passing through. Laser micromachining was conducted to process the center orifice for the development of coaxial catheter. To match the 0.9 mm-diameter housing, a 0.6 mm × 0.6 mm × 0.4 mm hollow acoustic stack (Figure 1B) was cut from the PZT-based stack using a dicing saw (ZHZZ-SD4800, DISCO Corporation, Japan). The aperture of the stack correlates with the transducer performance, while the thickness is critical in the transducer design. The thick stack could facilitate the wire connection and catheter fabrication, but induce less accuracy on the orifice diameter, which was micromachined by a focused laser beam with a big numerical aperture (NA). To show the effect of laser micromachining on the transducer performance, a square stack with the same dimensions but without being laser micromachined (referred as the homemade square stack) was prepared. Besides, a commercial PZT acoustic stack (Blatek Corporation, USA) with the same dimensions (referred as the commercial square stack) was purchased for comparison.

## 2.2 | Fabrication of coaxial catheter and system

The miniature intravascular photoacoustic catheter was fabricated as displayed in Figure 2. The ultrasound transducer with a center orifice was used to detect the photoacoustic and ultrasound signals reflected from the biological tissue, which could not be placed directly on the

inner wall of the housing to avoid electrical disconnection between the backing layer, matching layer, and housing. The positive electrode of the wire was firstly connected on the backing layer of the stack using the electrically conductive adhesive (E-solder), while the negative electrode of the wire was pressed on the inner wall of housing by the stack using the E-solder to ensure the electrical connection between the negative electrode, housing, and matching layer of the stack. The parylene was deposited as the second matching layer and the waterproofing layer. A naked multimode fiber without coating was inserted into the orifice of the transducer, which was with a 0.105 mm-diameter core. A customized 45° rod silver mirror with the diameter of 0.78 mm was assembled on the tip of the catheter for reflecting the laser beam and photoacoustic/ultrasound signals. A torsion coil (Tu's Cheng Fa, China) was inserted into the housing, facilitating the rotation scanning. All the components were fixed by the electrically insulating epoxy. To show the significance of coaxial catheter design, a noncoaxial catheter with the same configurations as our reported work [36] was developed using the commercial square stack for comparison.

The signal from the pulsed laser source was used to trigger the synchronization of data acquisition (DAQ), translation and rotation of the catheter. Simultaneously, the signal was also sent to a custom-made delay module to provide a 5- $\mu$ s delayed trigger signal for the ultrasound pluser/receiver (5073PR, Olympus) to form an ultrasound image. A pulsed Nd:YAG laser (Medical Technology [Shenzhen] Co., Ltd., China) was used for photoacoustic excitation. The fiber (MMJ\_S 105/125-0.9-1m-FC/APC,

Femto Technology [Xi'an] Co. Ltd.) with 0.22NA was used to deliver the laser energy through the slip-ring and then into the catheter. The hollow transducer was used to detect the photoacoustic and ultrasound signals from the biological tissue. Both photoacoustic and ultrasound signals were amplified (39 dB) in the pulser/receiver and then digitized with a DAQ board (ATS9325, Alazar Tech). The setup of the intravascular photoacoustic system was also similar to our previous work [33]. More detailed information on the coaxial system and data acquisition can be found in the published work.

## 2.3 | Preparation of ex vivo tissue

Ex vivo imaging experiment was conducted to further confirm the superiority of the coaxial catheter design. Figure 3 shows the tissue fixed in agar and the corresponding imaging section. A coronary artery was fixed in agar for the imaging experiment, which was dissected from a fresh porcine heart and soaked in the formalin for 24 h for fixation.

In general, the inflammation tissue could not be detected by photoacoustic imaging directly in atherosclerosis, because the optical absorption of the inflammation cells is very weak. The exogenous nanoprobe are usually employed for targeting the inflammation tissue [36–38]. Here, 1 ml solution of 1064-nm photoacoustic

nanoprobes (Supplementary information S1) were injected into the tissue near the artery wall (Figure 3B) to mimic the targeted cells. As the injected nanoprobe could outflow from the fresh tissue after immersed in water, the porcine heart tissue was preprocessed in the formalin and fixed in the agar to retain the nanoprobe in the designated location. The coaxial and noncoaxial catheters were inserted into the tube, respectively, for imaging nanoprobe. After the experiments, the vessel was cut and the cross section is shown in Figure 3C.

## 3 | RESULTS

### 3.1 | Optical simulation

To avoid tissue burns, the laser energy should be limited to a safe range. To investigate the optical fluence of different designs, simulations were conducted using the ZEMAX software. Figure 4 illustrates the schematics of laser beam irradiating from the noncoaxial and the coaxial catheter designs. The diameters of laser beam from different catheter designs along with the imaging distance were calculated as shown in Table 1. In addition, Figure 4 demonstrates the configuration of coaxial and noncoaxial catheters, in which optical parameters were set based on the previous work [33] and this work, respectively.

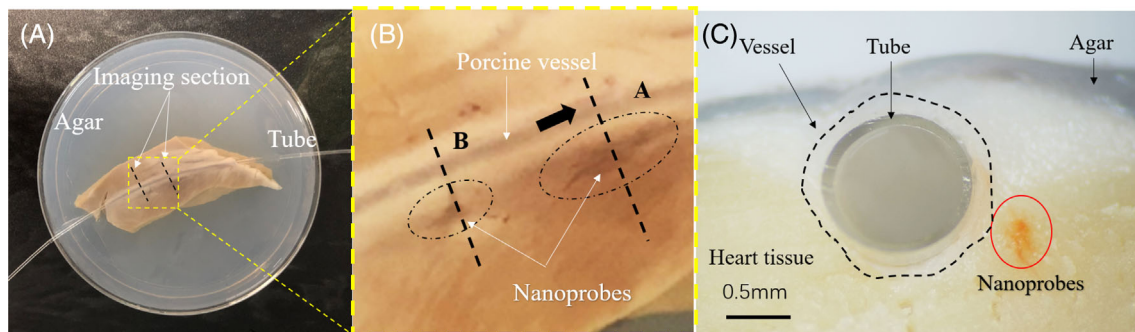


**FIGURE 3** (A) Photo of the ex vivo porcine heart tissue fixed in agar; (B) zoom-in image of a, indicating the imaging sections and the position of injected nanoprobe; (C) cross-sectional image in the viewing angle of black arrow in (B). Red circle indicates the position of injected nanoprobe. Black dash line shows the profile of porcine vessel

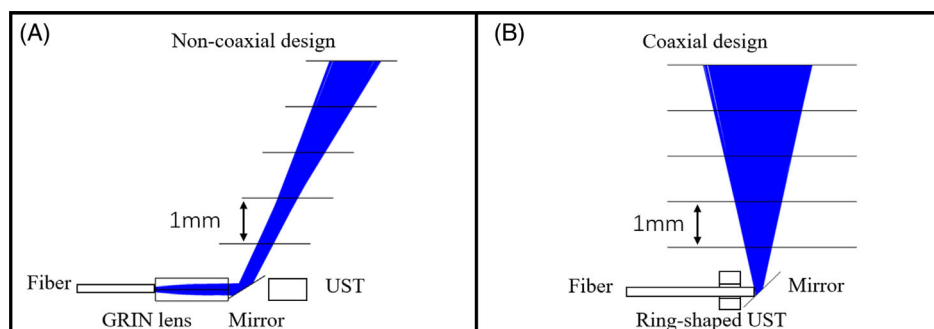


**FIGURE 4** Schematics of laser beam irradiating from the noncoaxial and the coaxial catheter designs. (A) Configuration of noncoaxial design; (B) configuration of coaxial design. GRIN lens, gradient-index lens; UST, ultrasound transducer

### 3.2 | Basic transducer performance

To evaluate the transducer performance, pulse-echo tests were performed on the transducers fabricated using the aforementioned acoustic stacks. The experimental setup was similar to our previous work [35, 39]. As shown in Figure 5, the transducer fabricated using the commercial square stack (Figure 5A) exhibited slightly higher frequency (34 MHz) when compared to the homemade square one (30 MHz). Its sensitivity was also better when compared to the homemade stacks (Figure 5B,C), which may be attributed to the variations in terms of stack design and materials. Although the laser micromachining process may not affect the macroscopic piezoelectric performance [40], the aperture size was reduced such that the hollow transducer would exhibit lower sensitivity but wider bandwidth than the transducer fabricated using the homemade square stack as shown in Figure 5C. The transducer properties including frequency, bandwidth, and echo amplitude are summarized in Table 2.

### 3.3 | Phantom imaging

A phantom was developed to evaluate the imaging performance of transducers with the coaxial and noncoaxial

**TABLE 1** Diameters of laser beam from different catheter designs along with the imaging distance

| Imaging distance (mm)      | 1   | 2    | 3    | 4    | 5    |
|----------------------------|-----|------|------|------|------|
| Diameter ( $\mu\text{m}$ ) |     |      |      |      |      |
| Noncoaxial design          | 440 | 540  | 774  | 1036 | 1312 |
| Coaxial design             | 640 | 1100 | 1560 | 2000 | 2400 |

designs, in which 50  $\mu\text{m}$ -diameter tungsten wires were distributed vertically with a 0.5 mm gap on a 3D-printed model (Figure 6A). During the imaging testing, the catheters moved horizontally to scan the tungsten wires in a water tank (Figure 6B). Figure 6C–F shows the dual-modality imaging results acquired from catheters with different designs. Figure 6C,D shows the photoacoustic and ultrasound images acquired from the coaxial catheter, in which both imaging depths were up to 5.7 mm. The noncoaxial catheter offered much brighter images due to the better sensitivity of commercial square stack, but its photoacoustic imaging depth was shorter than 2.5 mm as shown in Figure 6E,F. The results show that the coaxial catheter configuration could perform imaging on targets deeper than the noncoaxial one. Although the sensitivity was affected by the reduction of aperture size, the hollow transducer showed the potential of having sufficient sensitivity to detect the inner structure of the vessel.

It should be noted that the imaging started from  $-1$  mm using the coaxial catheter as shown in Figure 6C,D, which was the distance between the hollow transducer and the mirror center ( $\sim 1$  mm). On the other hand, the transducer is usually positioned on

**TABLE 2** Properties of transducers fabricated using different acoustic stacks

|                         | Frequency (MHz) | $-6$ dB bandwidth (%) | Peak-to-peak echo voltage (V) |
|-------------------------|-----------------|-----------------------|-------------------------------|
| Commercial square stack | 34              | 40                    | 3.54                          |
| Homemade square stack   | 30              | 40                    | 1.94                          |
| Hollow stack            | 35              | 60                    | 1.36                          |

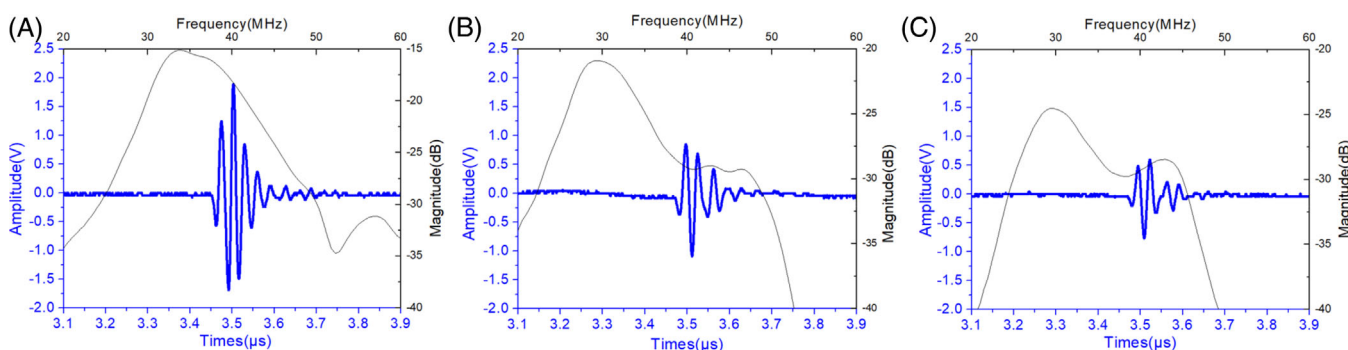


**FIGURE 5** Pulse-echo waveforms of ultrasound transducers fabricated using different acoustic stacks. (A) Commercial square stack, (B) homemade square stack, and (C) hollow stack

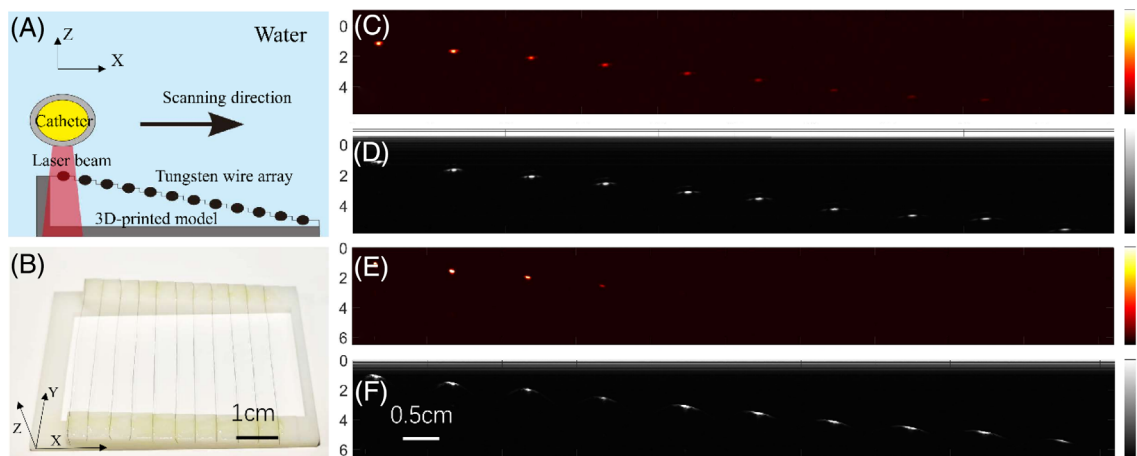


**FIGURE 6** Schematic, photo, and imaging results of tungsten wires in different depths acquired by the catheters with coaxial and noncoaxial designs. (A) Schematic of the imaging method; (B) photo of tungsten wire phantom. Photoacoustic and ultrasound images acquired using (C,D) the coaxial catheter and (E,F) the noncoaxial catheter. The photoacoustic and ultrasound images are displayed with the same normalized range, respectively

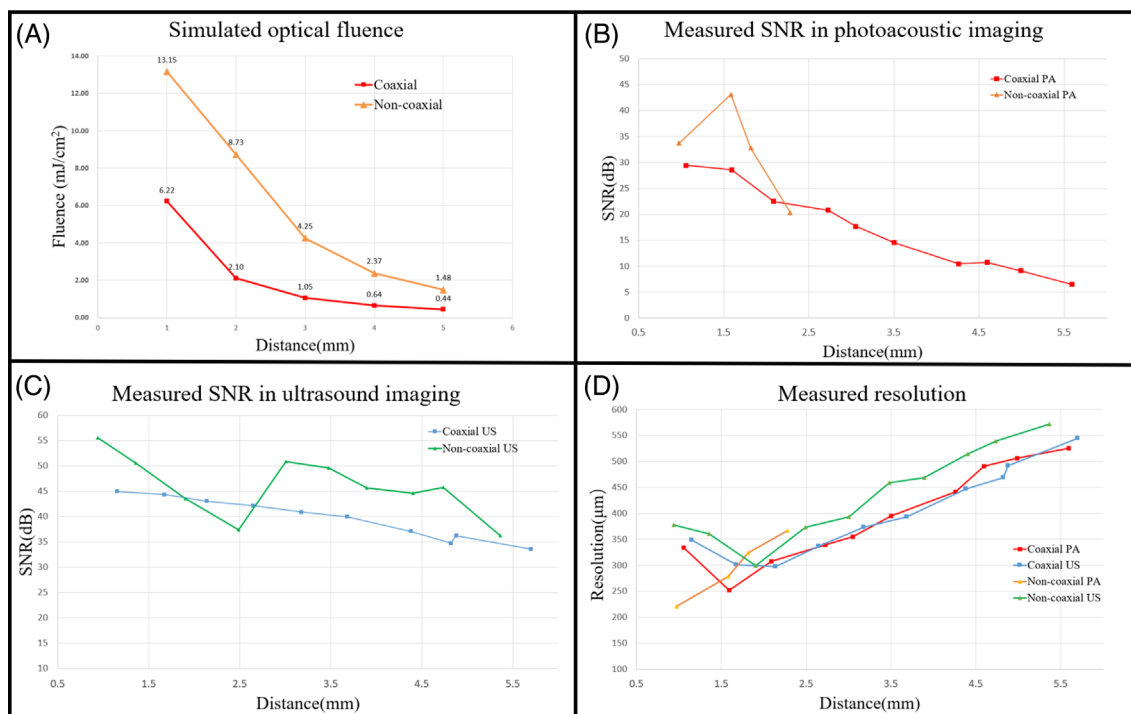


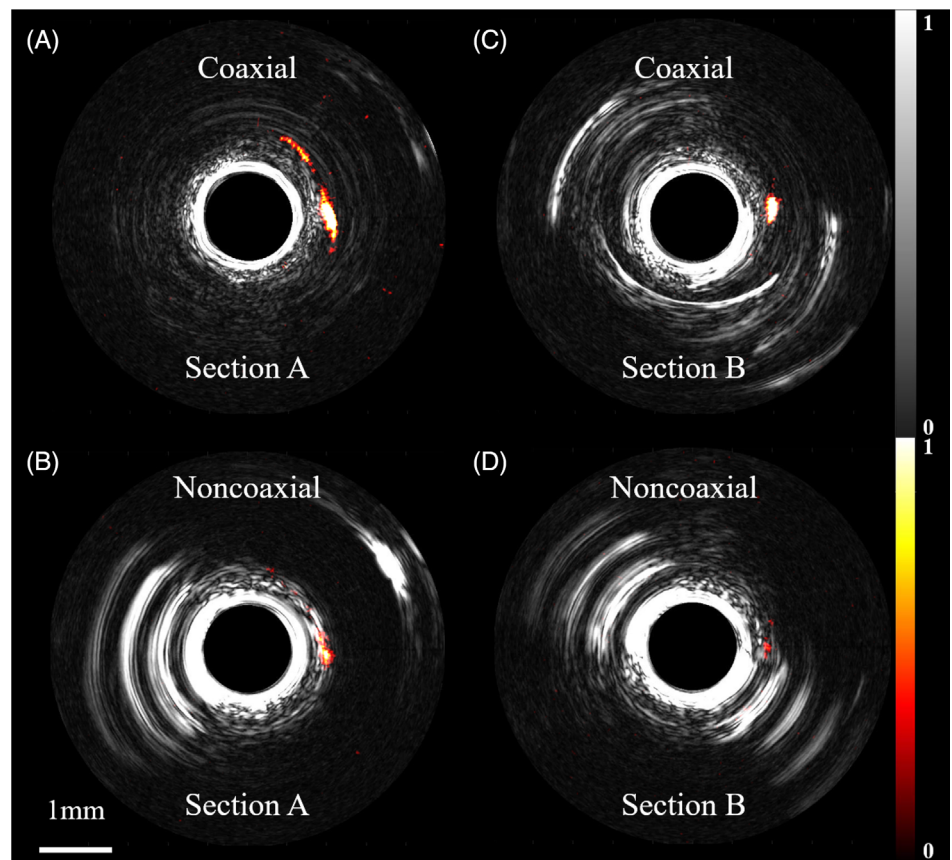
**FIGURE 7** Comparison of results against imaging distance for coaxial and noncoaxial catheter designs. (A) Simulated optical fluence; (B) measured SNR in photoacoustic imaging; (C) measured SNR in ultrasound imaging; (D) measured resolutions from Figure 6C–F

the axis of the housing with the noncoaxial configuration, facing the imaging window. The oblique illumination and side-view detection in the traditional noncoaxial design could cause signals missing in the area of the high-amplitude initial excitation signal. Thus, when compared to the noncoaxial catheter, the coaxial catheter could avoid the interference of initial excitation signals that is beneficial to imaging the nearer targets.

### 3.4 | Results of optical fluence, SNR and resolution

Figure 7 compares the simulated and measured results between coaxial and noncoaxial catheter designs. Figure 7A shows the variation of optical fluence calculated by the simulation results. In this study, the laser energy from the tip of the coaxial catheter was  $\sim 20 \mu\text{J}$  and the irradiation area at the depth of 1 mm was

**FIGURE 8** Ex vivo imaging results acquired by the catheters with coaxial and noncoaxial designs. Fused B-scan images of photoacoustic and ultrasound images of (A,B) section A and (C,D) section B. The photoacoustic and ultrasound images are displayed with the same normalized range, respectively



$\sim 440 \mu\text{m}$ , resulting in the optical fluence of  $\sim 6.22 \text{ mJ/cm}^2$  that meets the standard in accordance with the American National Standards Institute (ANSI). The difference in optical fluence was big between two designs at short distances but got smaller along with the increasing distance.

Figure 7B,C shows the measured results of SNR in photoacoustic and ultrasound imaging acquired by two different catheter designs, respectively, showing that the coaxial design is capable of imaging the targets with better SNR in long distance. Figure 7D demonstrates the imaging resolutions measured in Figure 6C–F.

### 3.5 | Ex vivo imaging

The catheter with a protective tube was inserted into the porcine coronary artery for photoacoustic imaging. Figure 8 shows the B-scan imaging results of two catheters, which are combined photoacoustic/ultrasound images of Sections A and B of the artery (Figure 3B). Figure 8A,C is fused images acquired by the coaxial catheter, in which the photoacoustic signal of the nanoprobe can be seen in the 2-mm depth. For the images acquired

from the noncoaxial catheter (Figure 8B,D), ultrasound signals reflected from the protective tube were very strong, which was due to the high sensitivity of the commercial square stack. All the images are displayed with the normalized range. The imaging experiment demonstrated that the coaxial catheter possessed superior imaging quality and depth.

## 4 | DISCUSSION

Atherosclerotic plaque and inflammation are the linchpin in the diagnosis of stroke and ischemic heart disease, which contribute from intima to adventitia. To reach the deeper imaging depth and meet the clinical operation, the simultaneous maximization of the light-sound overlap area and minimization of the catheter size is necessitated. Though some previous works [27–29] have been reported on the development of hollow transducers, the bulky devices cannot be inserted into the  $\sim 1 \text{ mm}$ -diameter vessel for intravascular imaging. A coaxial design [22, 30] based on the 3D-printed model was reported to collect the reflected signal from an optical fiber core, but the design could not cover the imaging window, leading to an apparent loss of signal.

To access the coronary artery, the intravascular catheter should be limited to 1 mm in diameter, which restricts the size of the transducer. The miniature hollow ultrasound transducer plays the pivotal role to combine the optical and acoustic beams coaxially, which was of higher significance than simply reducing the stack dimensions. First of all, the orifice diameter should be carefully designed to balance the fiber diameter and the detecting area. Second, the thickness of the acoustic stack should be limited to  $<0.5$  mm to compensate a micromachining error between the front and back of the orifice due to the big NA of the laser beam so as to minimize the area mismatching in each layer. Last but not least, to avoid the damage irradiated by the high-power laser during micromachining, the parylene coating must be done after the transducer fixation but before the fiber installation in the housing. All aforementioned factors should be taken into account in the fabrication process of coaxial catheters.

Transducer performance and optical fluence are key factors to acquire photoacoustic images with good SNR. The former factor is related to the properties of acoustic stack, while the latter one correlates with the laser energy and optical focusing. As shown in Figure 7A, the noncoaxial catheter offered better optical fluence due to the contribution of GRIN lens for laser beam focusing. Nevertheless, the coaxial catheter exhibited better performance in depth for both photoacoustic and ultrasound imaging (Figure 7B,C) because of having the larger light-sound overlap area. The fluctuation of signal acquired by the noncoaxial catheter was attributed to the distortion of tungsten wire.

The imaging resolutions of coaxial design were consistent with those of noncoaxial one, while the resolutions increased overall along with the imaging distance because both systems were dependent on the acoustic resolution, as shown in Figure 7D.

The catheter with the coaxial design provided better photoacoustic imaging in-depth than the noncoaxial one in both phantom and ex vivo imaging experiments. The photoacoustic imaging depth of tungsten wires acquired by the coaxial catheter reached  $>5$  mm (Figure 6C), and the porcine artery structure and the nanopores in the adventitia can be imaged with high sensitivity (Figure 8A,C). Though both the sensitivity of the commercial square stack and the optical fluence of the noncoaxial configuration were higher, the nanopores could not be fully imaged due to the limited light-sound overlap area in the noncoaxial catheter design (Figure 8B,D). All the results indicated that the coaxial catheter is capable of acquiring information from the intima to adventitia of the atherosclerotic artery.

Strong reflections are shown in Figure 8B,D, which is due to the noncoaxial design. The US transducer sat closely with the tube surface, which easily reflected the ultrasound signal from the inner surface of protective tube during rotation. Moreover, the sensitivity of commercial stack is higher, so the reflection would also be stronger. The material of the protective tube is the low-density polyethylene, which could be optimized by reducing the thickness for reducing the ultrasound reflection.

The promising potential of the coaxial catheter design was demonstrated, while there are still rooms to further improve the catheter performance and enhance the potential for clinical applications. For example, the imaging performance could be improved by employing better piezoelectric materials such as PMN-PT single crystal or corresponding 1–3 composite. Besides, the light beam could be collimated or optimized using some optical components to increase the optical fluence. The optimized laser beam can also improve the system's resolution. The coaxial design could also combine with other optical modalities using the same fiber, such as optical coherence tomography (OCT), to further strength the biomedical imaging capability.

## 5 | CONCLUSION

In summary, an intravascular photoacoustic catheter with coaxial excitation and detection was developed. The miniature hollow ultrasound transducer was successfully fabricated using laser micromachining. The detecting area of the transducer could fully cover the imaging window, receiving all signals reflected from a rod mirror. The phantom imaging results indicated that the proposed coaxial catheter design was able to detect the targets in a longer range of distance even with lower optical fluence when compared to the noncoaxial design. The ex vivo imaging results demonstrated that the coaxial catheter exhibited much better imaging depth than the noncoaxial one. The reduced catheter size and the improved performance of the coaxial intravascular photoacoustic catheter would be one step closer to clinical implementation for both plaque evaluation and molecular imaging.

## AUTHOR CONTRIBUTIONS

K.L. and X.G. initiated this investigation, supervised the project, and edited the paper. R.L. implemented the project, analyzed the data and wrote the paper. Q.Z. contributed the ultrasound transducer fabrication.

S.L. and J.Z. contributed to the animal preparation and ultrasound transducer test. X.W. contributed to the optical simulation and analysis. D.S. contributed to the preparation of piezoelectric materials and phantom.

## ACKNOWLEDGMENTS

This work was partially supported by National Key Research and Development Program of China (2018YFC0116300); National Natural Science Foundation of China (62005306, 61975226); CAS Key Laboratory of Health Informatics (2011DP173015); Guangdong Provincial Key Laboratory of Biomedical Optical Imaging Technology (2020B121201010); Hong Kong Research Impact Fund (R5029-19); Hong Kong Research Grants Council (15220920); Shenzhen Science and Technology Innovation Committee (ZDSY20130401165820357, JCYJ20200109114610201).

## CONFLICT OF INTEREST

The authors declare that there are no conflicts of interest related to this article.

## DATA AVAILABILITY STATEMENT

Data underlying the results presented in this paper are not publicly available at this time but may be obtained from the authors upon reasonable request.

## ORCID

Xiaojing Gong  <https://orcid.org/0000-0002-8221-3522>

Kwok-ho Lam  <https://orcid.org/0000-0003-1456-9049>

## REFERENCES

- [1] G. R. Geovanani, P. Libby, *Clin. Sci.* **2018**, *132*, 1243.
- [2] A. Gistera, G. K. Hansson, *Nat. Rev. Nephrol.* **2017**, *13*, 13.
- [3] B. Wang, J. L. Su, J. Amirian, S. H. Litovsky, R. Smalling, S. Emelianov, *Opt. Express* **2010**, *18*, 4889.
- [4] A. M. Sharma, A. Gupta, P. K. Kumar, J. Rajan, L. Saba, I. Nobutaka, J. R. Laird, A. Nicolades, J. S. Suri, *Curr. Atheroscl. Rep.* **2015**, *17*, 13.
- [5] P. Libby, *Arterioscl. Thromb. Vascul. Biol.* **2012**, *32*, 2045.
- [6] M. Back, A. Yurdagül, I. Tabas, K. Oorni, P. T. Kovanen, *Nat. Rev. Cardiol.* **2019**, *16*, 389.
- [7] M. G. Zhou, H. D. Wang, X. Y. Zeng, P. Yin, J. Zhu, W. Q. Chen, X. H. Li, L. J. Wang, L. M. Wang, Y. N. Liu, J. M. Liu, M. Zhang, J. L. Qi, S. C. Yu, A. Afshin, E. Gakidou, S. Glenn, V. S. Krish, M. K. Miller-Petrie, W. C. Mountjoy-Venning, E. C. Mullany, S. B. Redford, H. Y. Liu, M. Naghavi, S. I. Hay, L. H. Wang, C. J. L. Murray, X. F. Liang, *Lancet* **2019**, *394*, 1145.
- [8] M. J. Bom, D. J. van der Heijden, E. Kedhi, J. van der Heyden, M. Meuwissen, P. Knaapen, S. A. J. Timmer, N. van Royen, *Circul. Cardiovasc. Imag.* **2017**, *10*, 20.
- [9] Y. Li, Z. P. Chen, *Biomed. Eng. Lett.* **2018**, *8*, 193.
- [10] C. Stefanadis, C. K. Antoniou, D. Tsiachris, P. Pietri, *J. Am. Heart Assoc.* **2017**, *6*, 18.
- [11] R. Grabner, K. Lotzer, S. Dopping, M. Hildner, D. Radke, M. Beer, R. Spanbroek, B. Lippert, C. A. Reardon, G. S. Getz, Y. X. Fu, T. Hehlhans, R. E. Mebius, M. van der Wall, D. Kruspe, C. Englert, A. Lovas, D. S. Hu, G. J. Randolph, F. Weih, A. J. R. Habenicht, *J. Exp. Med.* **2009**, *206*, 233.
- [12] Y. Y. Liu, C. Liang, X. Liu, B. Liao, X. M. Pan, Y. S. Ren, M. Fan, M. Li, Z. Q. He, J. X. Wu, Z. G. Wu, *Atherosclerosis* **2010**, *208*, 34.
- [13] A. Milutinovic, D. Suput, R. Zorc-Pleskovic, *Bosnian J. Basic Med. Sci.* **2020**, *20*, 21.
- [14] M. Akhavanpoor, C. A. Gleissner, H. Akhavanpoor, F. Lasitschka, A. O. Doesch, H. A. Katus, C. Erbel, *Cardiovasc. Pathol.* **2018**, *32*, 8.
- [15] S. K. Mohanta, L. Peng, Y. Li, S. Lu, T. Sun, L. Carnevale, M. Perrotta, Z. Ma, B. Förstera, K. J. N. Stanic, *Nature* **2022**, *605*, 152.
- [16] Y. C. Cao, A. Kole, J. Hui, Y. Zhang, J. Y. Mai, M. Alloosh, M. Sturek, J. X. Cheng, *Sci. Rep.* **2018**, *8*, 10.
- [17] S. Iskander-Rizk, M. Wu, G. Springeling, H. M. M. van Beusekom, F. Mastik, M. T. Hekkert, R. Beurskens, A. Hoogendoorn, E. M. J. Hartman, A. F. W. van der Steen, J. J. Wentzel, G. van Soest, *Eurointervention* **2019**, *15*, 452.
- [18] S. Sethuraman, J. H. Amirian, S. H. Litovsky, R. W. Smalling, S. Y. Emelianov, *Opt. Express* **2008**, *16*, 3362.
- [19] B. Wang, E. Yantsen, T. Larson, A. B. Karpouk, S. Sethuraman, J. L. Su, K. Sokolov, S. Y. Emelianov, *Nano Lett.* **2009**, *9*, 2212.
- [20] P. Lei, X. Wen, L. Wang, P. F. Zhang, S. H. Yang, *Opt. Lett.* **2019**, *44*, 5406.
- [21] X. Li, W. Wei, Q. F. Zhou, K. K. Shung, Z. P. Chen, *J. Biomed. Opt.* **2012**, *17*, 6.
- [22] Z. L. Piao, T. Ma, J. W. Li, M. T. Wiedmann, S. H. Huang, M. Y. Yu, K. K. Shung, Q. F. Zhou, C. S. Kim, Z. P. Chen, *Appl. Phys. Lett.* **2015**, *107*, 4.
- [23] M. Wu, G. Springeling, M. Lovrak, F. Mastik, S. Iskander-Rizk, T. S. Wang, H. M. M. van Beusekom, A. F. W. van der Steen, G. Van Soest, *Biomed. Opt. Express* **2017**, *8*, 943.
- [24] K. Jansen, M. Wu, A. F. van der Steen, G. J. O. E. van Soest, *Opt. Express* **2013**, *21*, 21472.
- [25] K. Jansen, A. F. van der Steen, M. Wu, H. M. van Beusekom, G. Springeling, X. Li, Q. Zhou, K. K. Shung, D. P. de Kleijn, G. van Soest, *J. Biomed. Opt.* **2014**, *19*, 026006.
- [26] K. Jansen, M. Wu, A. F. van der Steen, G. J. P. van Soest, *Photoacoustics* **2014**, *2*, 12.
- [27] W. Wei, X. Li, Q. F. Zhou, K. K. Shung, Z. P. Chen, *J. Biomed. Opt.* **2011**, *16*, 6.
- [28] P. Wang, T. Ma, M. N. Slipchenko, S. S. Liang, J. Hui, K. K. Shung, S. Roy, M. Sturek, Q. F. Zhou, Z. P. Chen, J. X. Cheng, *Sci. Rep.* **2014**, *4*, 7.
- [29] J. Y. Xiao, Y. N. Li, W. T. Jin, K. Peng, Z. Q. Zhu, B. Wang, *Appl. Opt.* **2016**, *55*, 2301.
- [30] J. Hui, Y. C. Cao, Y. Zhang, A. Kole, P. Wang, G. L. Yu, G. Eakins, M. Sturek, W. B. A. Chen, J. X. Cheng, *Sci. Rep.* **2017**, *7*, 11.
- [31] Y. C. Cao, J. Hui, A. Kole, P. Wang, Q. H. Yu, W. B. Chen, M. Sturek, J. X. Cheng, *Sci. Rep.* **2016**, *6*, 8.
- [32] R. N. MacAlpin, A. S. Abbasi, J. H. Grollman Jr., L. J. R. Eber, *Radiology* **1973**, *108*, 567.
- [33] Y. Li, R. Q. Lin, C. B. Liu, J. H. Chen, H. D. Liu, R. Q. Zheng, X. J. Gong, L. Song, *J. Biophoton.* **2018**, *11*, 8.
- [34] K. H. Lam, Y. Li, Y. Li, H. G. Lim, Q. Zhou, K. K. Shung, *Sci. Rep.* **2016**, *6*, 1.
- [35] Q. Zhang, X. M. Pang, Z. Q. Zhang, M. Su, J. H. Hong, H. R. Zheng, W. B. Qiu, K. H. Lam, *IEEE Trans. Ultrason. Ferroelectr. Freq. Control* **2019**, *66*, 1102.

- [36] Z. Xie, C. Shu, D. Yang, H. Chen, C. Chen, G. Dai, K. H. Lam, J. Zhang, X. Wang, Z. Sheng, D. Gao, C. Liu, L. Song, X. Gong, *Biomed. Opt. Exp.* **2020**, *11*, 6721.
- [37] A. P. Regensburger, E. Brown, G. Krönke, M. J. Waldner, F. J. B. Knieling, *Biomedicines* **2021**, *9*, 483.
- [38] Z. Jiang, X. Geng, L. Su, A. Chen, Z. Sheng, T. Jiang, *Mater. Today Chem.* **2022**, *26*, 101062.
- [39] K. H. Lam, H. F. Ji, F. Zheng, W. Ren, Q. Zhou, K. K. Shung, *Ultrasonics* **2013**, *53*, 1033.
- [40] K. H. Lam, Y. Chen, K. Au, J. Chen, J. Y. Dai, H. S. Luo, *Mater. Res. Bull.* **2013**, *48*, 3420.

## SUPPORTING INFORMATION

Additional supporting information can be found online in the Supporting Information section at the end of this article.

**How to cite this article:** R. Lin, Q. Zhang, S. Lv, J. Zhang, X. Wang, D. Shi, X. Gong, K. Lam, J. *Biophotonics* **2023**, *16*(4), e202200269. <https://doi.org/10.1002/jbio.202200269>